Bacterial flagellar motor PL-ring disassembly subcomplexes are widespread and ancient

Mohammed Kaplan[a], Michael J. Sweredoski[a], João P. G. L. M. Rodrigues[b], Elitza I. Tocheva[a,1], Yi-Wei Chang[a,2], Davi R. Ortega[a], Morgan Beeby[a,3], and Grant J. Jensen[a,c,4]

[a]Division of Biology and Biological Engineering, California Institute of Technology, Pasadena, CA 91125; [b]Department of Structural Biology, Stanford University, Stanford, CA 94305; and [c]Howard Hughes Medical Institute, California Institute of Technology, Pasadena, CA 91125

Edited by Jody W. Deming, University of Washington, Seattle, WA, and approved February 24, 2020 (received for review September 28, 2019)

The bacterial flagellum is an amazing nanomachine. Understanding how such complex structures arose is crucial to our understanding of cellular evolution. We and others recently reported that in several Gammaproteobacterial species, a relic subcomplex comprising the decorated P and L rings persists in the outer membrane after flagellum disassembly. Imaging nine additional species with cryo-electron tomography, here, we show that this subcomplex persists after flagellum disassembly in other phyla as well. Bioinformatic analyses fail to show evidence of any recent horizontal transfers of the P- and L-ring genes, suggesting that this subcomplex and its persistence is an ancient and conserved feature of the flagellar motor. We hypothesize that one function of the P and L rings is to seal the outer membrane after motor disassembly.

cryo-electron tomography | flagellar motor | evolution

The bacterial flagellum is one of the most famous macromolecular machines, made up of thousands of protein subunits that self-assemble in a highly synchronized manner into a motor, a flexible hook, and a long extracellular filament that rotates in a propeller-like fashion to move the cell (1). The process of how these different parts assemble has been studied extensively by using different biophysical and biochemical methods (2–7). These studies have resulted in the current "inside-out" model, which starts with the assembly of an inner-membrane-embedded type III secretion system (T3SS) export apparatus, a membrane/supramembrane (MS) ring, a cytoplasmic switch complex (aka C ring), and a periplasmic rod which connects the MS ring to the extracellular hook. The P (peptidoglycan) and L (lipopolysaccharide) rings surround the rod in the periplasm and are thought to act as a bushing during rotation. Finally, the hook is connected by junction proteins to the long filament. While almost all species have this conserved core, different species can have additional cytoplasmic, periplasmic, and extracellular components (8–12). For example, in some species (like *Vibrio* species [spp.]), the P and L rings are decorated by five proteins (MotX, MotY, FlgO, FlgP, and FlgT) (13, 14). In other species, like *Legionella pneumophila* and *Pseudomonas aeruginosa*, the P ring is decorated by a ring formed by MotY (9).

Much less is known about the process of flagellar disassembly, though it is known that *Caulobacter crescentus* loses its flagellum and pili at a specific stage of its life cycle (15). We and others also recently reported that different Gammaproteobacteria species lose their flagella when starving or due to mechanical stress (7, 16–18). Interestingly, in situ imaging using cryo-electron tomography (cryo-ET) showed that this disassembly process leaves an outer-membrane-associated relic subcomplex consisting of the decorated flagellar P and L rings (referred to henceforth as PL-subcomplexes). These PL-subcomplexes plug the hole in the outer membrane that might otherwise be present after the flagellum disassembles. However, it remains unclear whether these PL-subcomplexes only persist in Gammaproteobacteria, or if the phenomenon is more widespread.

Here, using a combination of cryo-ET (19) and subtomogram averaging (20, 21), we show that the PL-subcomplex persists in nine additional bacterial species, including *Vibrio cholerae*, *Vibrio harveyi*, and *Vibrio fischeri* (Gammaproteobacteria with sheathed flagella); *Hyphomonas neptunium*, *Agrobacterium tumefaciens*, and *C. crescentus* (Alphaproteobacteria); *Hylemonella gracilis* (Betaproteobacterium); *Campylobacter jejuni* (Epsilonproteobacterium); and *Acetonema longum* (Firmicute). Bioinformatics analyses further show that the P- and L-ring genes are ancient and diverged separately in each species (were not recently transferred horizontally). Together, these results suggest that the outer-membrane-sealing role of the PL-subcomplexes is ancient and widely conserved.

Results

To examine the generality of PL-subcomplex persistence and how the presence of a membranous sheath surrounding the flagellum might affect this process, we used cryo-ET to image nine additional bacterial species from five classes (Fig. 1). All previously described PL-subcomplex subtomogram averages have been of species with unsheathed flagella: *Shewanella oneidensis*, *L. pneumophila*, *P. aeruginosa*, *Salmonella enterica*, and *Plesiomonas shigelloides* (7, 16, 17) (*SI Appendix*, Fig. S1). All of these feature a crater-like structure in the outer membrane (see examples in *SI Appendix*, Fig. S1), sealed across the bottom by either the P- or L-ring proteins or additional, as-yet-unidentified molecules. This presumably is to avoid an ∼20-nm pore in the outer membrane, which might be detrimental to the cell. For this reason, we were

Significance

In order to understand the evolution of complex biological machines like the bacterial flagellar motor, it is crucial to know what each component does and when it arose. Here, we show that a subcomplex of the motor thought to act as a bushing for the spinning motor likely also serves another function—it plugs the hole in the outer membrane left when the flagellum disassembles. Moreover, this component and function is ancient, since it appears in diverse phyla without evidence of recent gene transfer.

Author contributions: M.K. and G.J.J. designed research; M.K., M.J.S., J.P.G.L.M.R., E.I.T., Y.-W.C., D.R.O., and M.B. performed research; M.K. and G.J.J. contributed new reagents/analytic tools; M.K., M.J.S., and G.J.J. analyzed data; and M.K. and G.J.J. wrote the paper.

The authors declare no competing interest.

This article is a PNAS Direct Submission.

[1]Present address: Department of Microbiology and Immunology, Life Sciences Institute, The University of British Columbia, Vancouver, BC V6T 1Z3, Canada.

[2]Present address: Department of Biochemistry and Biophysics, Perelman School of Medicine, University of Pennsylvania, Philadelphia, PA 19104.

[3]Present address: Department of Life Sciences, Imperial College London, South Kensington Campus, SW7 2AZ London, United Kingdom.

[4]To whom correspondence may be addressed. Email: jensen@caltech.edu.

This article contains supporting information online at https://www.pnas.org/lookup/suppl/doi:10.1073/pnas.1916935117/-/DCSupplemental.

First published April 2, 2020.

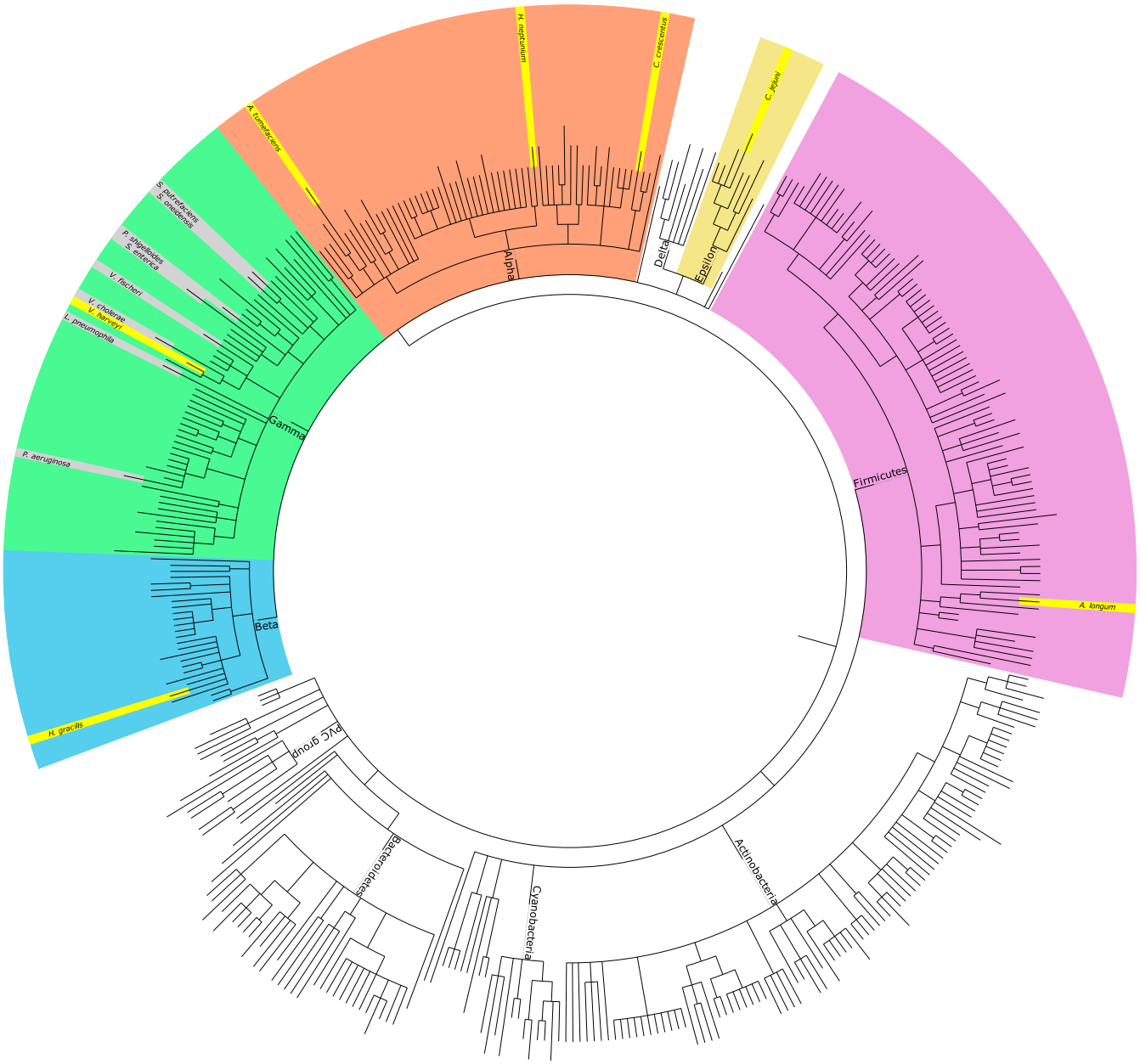

Fig. 1. A taxonomic tree of representative bacterial species. The species where PL-subcomplexes were previously reported are highlighted in gray (all in the Gammaproteobacteria class), while species with PL-subcomplexes identified in this study are highlighted in yellow. PVC, Planctomycetes–Verrucomicrobia–Chlamydiae.

first interested in whether there would be similar discontinuities in the outer membrane in species with sheathed flagella (in which the flagellum does not always penetrate the outer membrane). Images of individual PL-subcomplexes in *V. cholerae* and *V. fischeri* have been published (16), but no subtomogram averages are available. Thus, we first imaged the three Gammaproteobacterial species *V. cholerae*, *V. harveyi*, and *V. fischeri*, whose flagella are sheathed. As expected, we observed that the outer membrane of all three *Vibrio* species bent and extended to sheath the micrometers-long extracellular flagellar filaments (Fig. 2 *A*–*C*). At the base of these filaments, flagellar motors were clearly visible. Next to the fully assembled motors, we occasionally observed PL-subcomplexes (Fig. 2 *D*–*F*). Subtomogram averages of these subcomplexes confirmed that they indeed consisted of the embellished P and L rings (Fig. 2 *G*–*I*). In contrast to the structures previously observed from unsheathed flagella, the *Vibrio* spp. structures reported here exhibit an intact, convex outer-membrane layer across the top (Fig. 2 *G*–*I*). The bottom of the PL-subcomplex is still plugged, however (Fig. 2 *G*–*I*, yellow arrows), raising the question of why.

In addition, the structure of the PL-subcomplex in *V. harveyi* has an extracellular ring located just above the outer membrane (Fig. 2*I*, blue arrows). Such a ring is also present in the fully assembled sheathed flagellum (*SI Appendix*, Fig. S2, blue arrows). However, while the diameter of this ring is 30 nm in the PL-subcomplex, it has a diameter of 36 nm in the fully assembled flagellum, suggesting that this ring collapses upon flagellar disassembly. The presence of extracellular rings has been described in the unsheathed flagellum of *S. oneidensis* (9) and the sheathed flagellum of *Vibrio alginolyticus* (22). Importantly, the structure

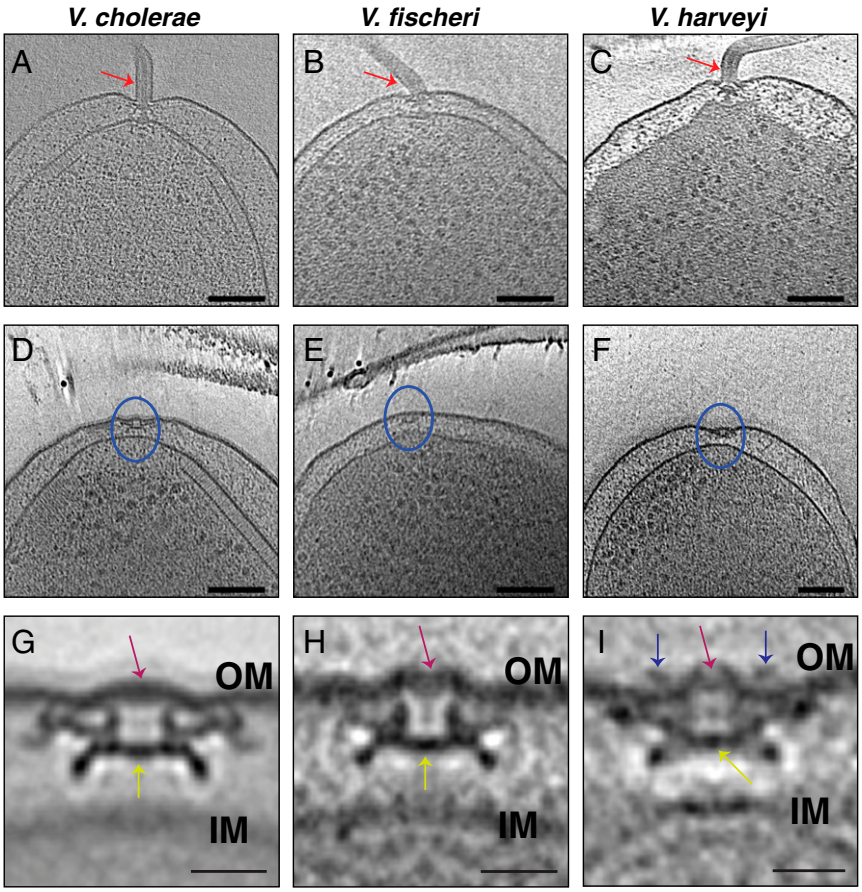

Fig. 2. Cryo-ET of the sheathed Gammaproteobacteria *Vibrio* species. (*A*–*C*) Slices through electron cryo-tomograms of *V. cholerae* (*A*), *V. fischeri* (*B*), and *V. harveyi* (*C*), highlighting the presence of a single polar sheathed flagellum in the three species (red arrows). (Scale bars: 100 nm.) (*D*–*F*) Slices through electron cryo-tomograms of *V. cholerae* (*D*), *V. fischeri* (*E*), and *V. harveyi* (*F*), highlighting the presence of flagellar disassembly PL-subcomplexes (blue circles). (Scale bars: 100 nm.) (*G*–*I*) Central slices through subtomogram averages of PL-subcomplexes in *V. cholerae* (*G*), *V. fischeri* (*H*), and *V. harveyi* (*I*). Purple arrows highlight the presence of intact outer membrane (OM) above the PL-subcomplexes. Yellow arrows indicate the proteinaceous plug inside the P ring. Blue arrows in *I* highlight the presence of an extracellular ring density in the average of *V. harveyi*. (Scale bars: 20 nm.) IM, inner membrane.

of the PL-subcomplex from *S. oneidensis* has an extra density located just at the membranous discontinuity resulting from disassembling the flagellum (*SI Appendix*, Fig. S1*A*). This density in *S. oneidensis* may also be due to the collapse of the extracellular ring present in the fully assembled flagellum.

After this comparison of the PL-subcomplexes in the sheathed and unsheathed flagella of Gammaproteobacteria, we were interested in whether PL-subcomplexes are specific to Gammaproteobacteria or present in other classes in the Proteobacteria phylum. We therefore examined five more species: *H. neptunium*, *A. tumefaciens*, and *C. crescentus* (Alphaproteobacteria [Fig. 3 *A*–*L*]); *H. gracilis* (Betaproteobacterium [Fig. 4 *A*–*D*]); and *C. jejuni* (Epsilonproteobacterium [Fig. 4 *E* and *F*]). PL-subcomplexes were observed in all of these species with the characteristic discontinuity in the outer membrane and a clear plugged base similar to their Gammaproteobacterial counterparts (not enough examples of *C. jejuni* PL-subcomplexes were available to unambiguously assign the presence of a plug). In *C. jejuni*, an inner-membrane-associated subcomplex of the flagellar motor (constituting the MS and C rings, the export apparatus, and the proximal rod) was present in the vicinity of the PL-subcomplex in a pattern reminiscent of what has recently been reported in *L. pneumophila* (7) (Movie S1 and *SI Appendix*, Fig. S3).

Having established that PL-subcomplexes are widespread in Proteobacteria, we next looked for them in *A. longum,* a diderm belonging to the class of Clostridia in the Firmicutes phylum. PL-subcomplexes were found in *A. longum* as well (Fig. 4 *G* and *H*).

The presence of PL-subcomplexes in diverse bacterial phyla could be because it is an ancient and conserved feature or because the P- and L-ring proteins were recently horizontally transferred. To explore these possibilities, we performed an implicit phylogenetic analysis on all species in which PL-subcomplexes have been found (by cryo-ET: 15 in total, including the species described here, plus those in refs. 7, 16, and 17). We compared the sequence distances among FlgI (P ring) and among FlgH (L ring) orthologs, as well as 25 single-copy well-conserved proteins (as described in ref. 23; *SI Appendix*, Table S1). This allowed us to investigate how P- and L-ring proteins evolved compared to the reference 25 proteins (24). If the sequence distances among FlgI (or FlgH) proteins in two species is smaller than the 25 reference proteins, this indicates a horizontal gene-transfer event (24). This analysis of pairwise comparisons of the investigated species showed that the sequence distances between FlgH proteins was at least as divergent as the 25 reference proteins, and, therefore, there is no evidence of horizontal gene transfer between these species (Fig. 5*A* and *SI Appendix*, Table S2). This same result was seen for FlgI (Fig. 5*B* and *SI Appendix*, Table S3). For the minimum and average protein

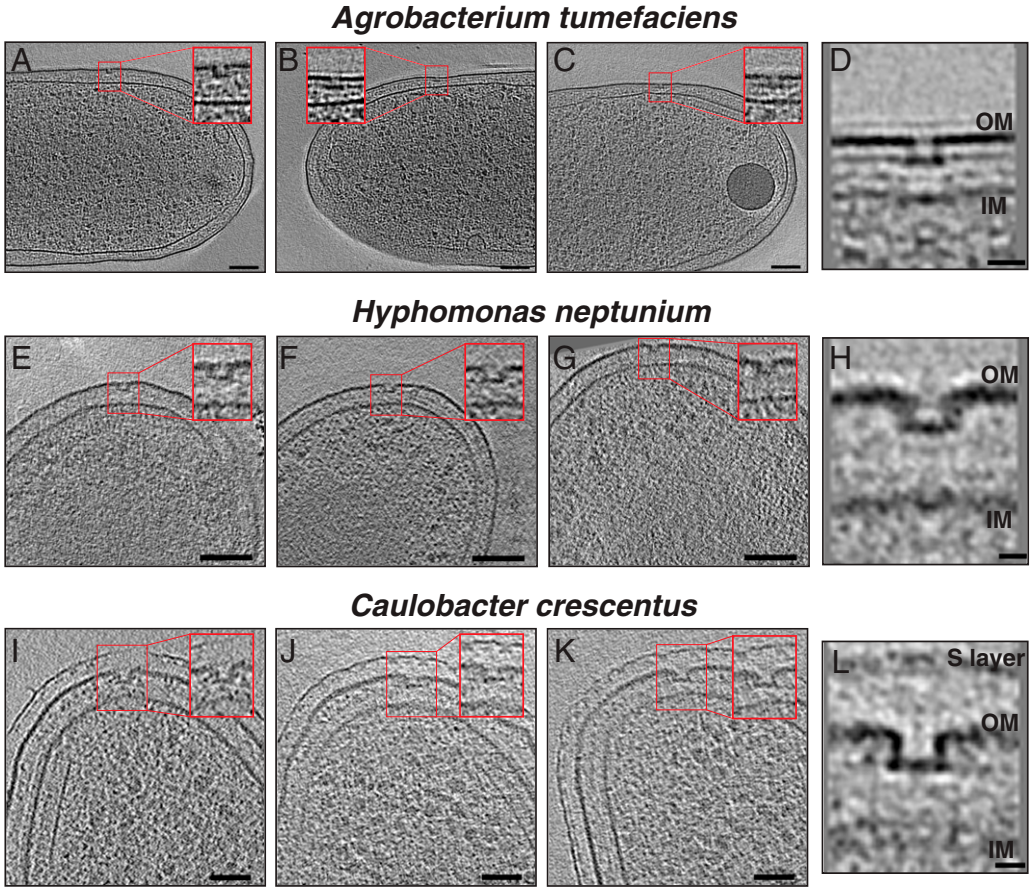

Fig. 3. Cryo-ET of the Alphaproteobacteria species. (*A–C*) Slices through electron cryo-tomograms of *A. tumefaciens* highlighting the presence of flagellar disassembly PL-subcomplexes with zoom-ins (*Insets*) of these subcomplexes present in the red squares. (Scale bars: 100 nm.) (*D*) Central slice through a subtomogram average of PL-subcomplexes in *A. tumefaciens*. (Scale bar: 20 nm.) (*E–G*) Same as in *A–C*, but for *H. neptunium*. (Scale bars: 100 nm.) (*H*) Central slice through a subtomogram average of PL-subcomplexes in *H. neptunium*. (Scale bar: 10 nm.) (*I–K*) Same as in *A–C*, but for *C. crescentus*. (Scale bars: 50 nm.) (*L*) Central slice through a subtomogram average of PL-subcomplexes in *C. crescentus*. (Scale bar: 10 nm.) IM, inner membrane; OM, outer membrane.

distances among the 15 species in this study, see *SI Appendix*, Table S4.

In *Shewanella putrefaciens* and *P. shigelloides*, two copies for FlgI and FlgH were annotated. For both species and both genes, one copy showed more similarity to the nearest relative (*S. putrefaciens* FlgI, A4Y8M8, and FlgH, A4Y8M9; *P. shigelloides* FlgI, R8AUG5, and FlgH, R8AUH3, referred to as the primary copy). On the other hand, the other copy (referred to as the secondary copy) showed more divergence from any studied organism (*S. putrefaciens* FlgI, A4YB38, and FlgH, A4YB39; *P. shigelloides* FlgI, R8AS48, and FlgH, R8AS34; *SI Appendix*, Figs. S4 and S5 and Tables S5 and S6). GC-content analysis provided no evidence that any copy of FlgI and FlgH in either species is a result of horizontal gene transfer (*SI Appendix*, Figs. S6 and S7 and *Materials and Methods*).

Discussion

An important step in reconstructing the evolutionary history of biomolecular complexes is to know when certain features and functions originated. Recent studies indicate that the bacterial flagellum, one of the prime motility nanomachines in the prokaryotic world, is an ancient machine that originated from a single or few proteins through multiple gene-duplication and diversification events that preceded the common ancestor of bacteria (23). Some parts of the flagellar system are homologous to other subcomplexes present in other machines. The stator proteins MotA/B are homologous to proteins in the Tol-Pal and TonB systems, while the motor's ATPase is homologous to the beta subunit of the adenosine triphosphate synthase (23, 25). This suggests that other, even older machines donated features and functions to the first motor. Moreover, the T3SS, also known as the injectisome, is homologous to the bacterial flagellum (though the P and L rings of the motor are not homologous to the secretin part of the injectisome) (26). Because motility preceded the evolution of eukaryotic cells, the targets of T3SS, and the T3SS is restricted mainly to proteobacteria, the injectisome likely derived from the flagellum (27, 28). On the other hand, motility in the archaeal domain of life is driven by another nanomachine—namely, the archaellum, which is structurally related to the type-IV pilus system and not to the bacterial flagellum, suggesting different evolutionary histories for these motility nanomachines (29–31).

The proteins that form the P and L rings—namely, FlgI and FlgH, respectively—are present widely in flagellated bacteria; however, they are not as universal as other flagellar proteins known as the core proteins. For example, Spirochaetes (characterized by periplasmic flagella) and Firmicutes (many of its members are characterized by a single membrane) do not necessarily have the P and L rings. These two phyla are usually considered among the earliest evolved phyla of bacteria (32), suggesting that, although the P and L rings appeared early during the flagellar evolution, they were probably not present at first (23). However, recent studies prompted a proposal that the diderm cell plan may represent a permanent stall in one phase of

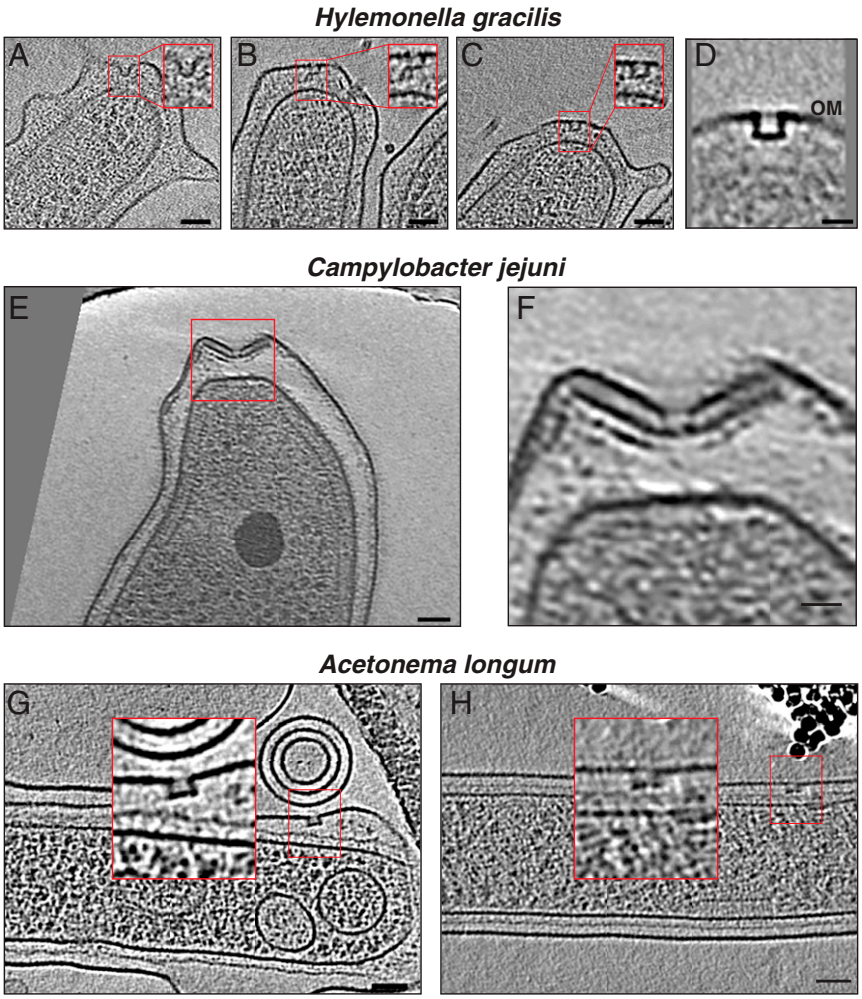

Fig. 4. Cryo-ET of Betaproteobacteria, Epsilonproteobacteria, and Firmicutes. (*A*–*C*) Slices through electron cryo-tomograms of *H. gracilis* highlighting the presence of flagellar disassembly PL-subcomplexes with zoom-ins (*Insets*) of these subcomplexes present in the red squares. (Scale bars: 50 nm.) (*D*) Central slice through a subtomogram average of PL-subcomplexes in *H. gracilis*. (Scale bar: 20 nm.) (*E*) A Slice through electron cryo-tomogram of *C. jejuni* highlighting the presence of a flagellar disassembly PL-subcomplex (red square). (Scale bar: 50 nm.) (*F*) A zoom-in of the area enclosed in the red square in *E*. (Scale bar: 20 nm.) (*G* and *H*) Slices through electron cryo-tomograms of *A. longum* highlighting the presence of flagellar disassembly PL-subcomplexes with zoom-ins (*Insets*) of these subcomplexes present in the red squares. (Scale bars: 50 nm.)

sporulation and that the last common ancestor of all existing bacteria was a diderm sporulator. This model means that modern monoderms descended from a diderm that lost its outer membrane (33, 34). This hypothesis is not unreasonable in light of cataclysmic conditions of early Earth, in which only a spore might have been able to persist through some evolutionary bottleneck. All this makes the origin of PL rings very speculative. Perhaps the flagellum did evolve before diderms, implying that PL rings evolved later than other flagellar components. Alternatively, the flagellum might not have evolved until there were already diderms around, suggesting that PL rings might be as equally ancient as other flagellar parts.

While other periplasmic and extracellular components of the flagellum (the proximal and distal rods, the hook, the hook–filament junction proteins, and the filament proteins) are exported by the flagellar T3SS export apparatus, the P- and L-ring proteins are secreted through the Sec pathway (35). Also, previous studies suggested that the secreted FlgI and FlgH proteins can exist in a stable form in the periplasm before their nucleation on the rod, which could be either due to high intrinsic stability of these two proteins or due to the low protease activity in the periplasm (2, 36). This might also explain the persistence of plugged PL-subcomplexes after flagellar disassembly. Alternatively, although the P and L rings have been thought to act as bushings supporting the rotation of the rod, the discovery that they persist in an altered, sealed form after the disassembly process could suggest an additional function—perhaps they remain to seal what would otherwise be a hole in the outer membrane. Here, we have found that PL-subcomplexes are widespread among bacteria and ancient (not the result of recent horizontal gene transfers). This indicates that the putative outer-membrane-sealing function is important enough to have been conserved since the diversification of bacterial phyla.

In addition, we showed that, in species with sheathed flagella, the outer membrane remained intact above PL-subcomplexes, but the base of the PL-subcomplexes was, nevertheless, apparently sealed. This raises questions about the nature and function of the PL-subcomplex in these species. Does it serve a function distinct from membrane-sealing in *Vibrio*, or it could be a vestige retained in their evolution from ancestors with unsheathed flagella? Finally, it will be interesting to find out whether membrane seals are needed only for flagellum disassembly, or if they might be needed in other closely related systems like the injectisome.

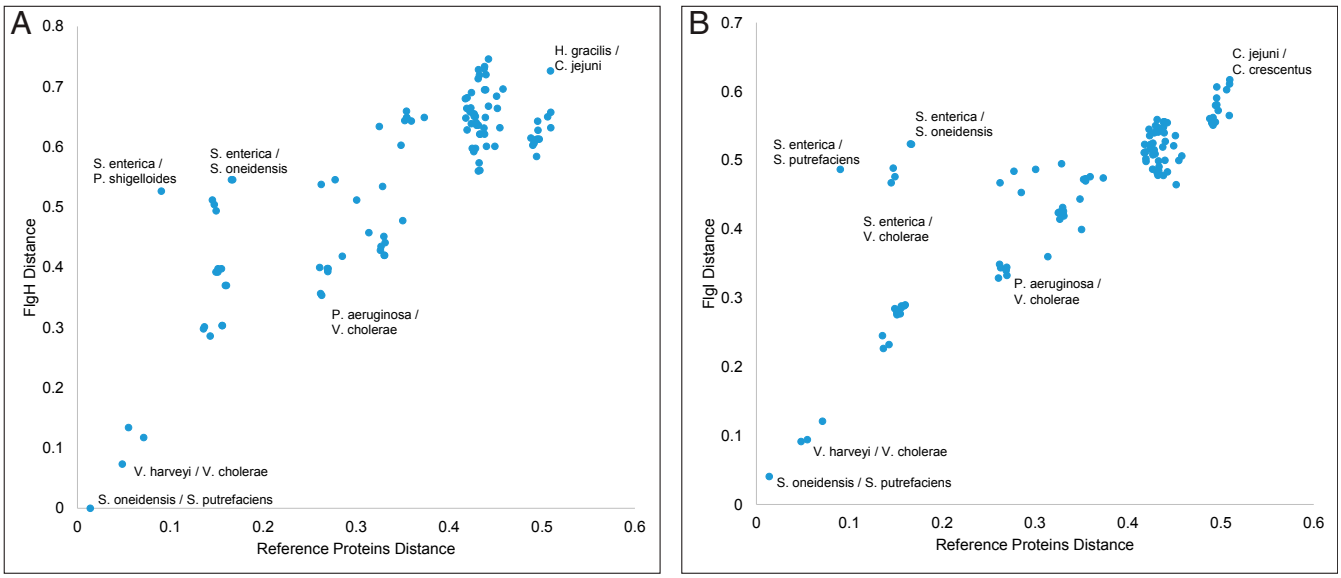

Fig. 5. Implicit phylogenetic analysis of bacterial L- and P-ring proteins. (*A*) A scatter plot of pairwise sequence distance of the 15 investigated species in this study based on concatenated 25 reference proteins and the L-ring protein FlgH. Some examples of pairwise species comparisons are annotated in the plot for the sake of clarity. (*B*) Same as in *A*, but with the P-ring protein FlgI. Plots shown in *A* and *B* are made with the primary copies of *P. shigelloides* and *S. putrefaciens* FlgI and FlgH proteins. For similar plots with the secondary copies of FlgI and FlgH in these two species, see *SI Appendix*, Figs. S4 and S5. The *x* and *y* axes in these plots have arbitrary units.

Materials and Methods

Cell Types and Growth Conditions. *V. cholerae* was grown 24 h in Luria–Bertani (LB) medium at 30 °C, diluted 150 μL into 2 mL of Ca–Hepes buffer, and grown at 30 °C for another 16 h. *V. harveyi* was grown in agrobacterium (AB) medium overnight at 30 °C. *V. fischeri* was grown overnight at 28 °C in salt-supplemented LB medium with 35 mM $MgSO_4$ (as described in ref. 37). Wild-type *A. tumefaciens* C58 was transformed with Ti plasmid encoding for VirB8 fluorescently tagged with green fluorescent protein (GFP). Cells were grown overnight in LB at 28 °C and subsequently spun down and resuspended to an optical density at a wavelength of 600 nm (OD_{600}) = 0.1 in AB medium supplemented with 300 μg/mL streptomycin and 100 μg/mL spectinomycin. The cells were switched to 19 °C and grown for 5 h. To induce expression of VirB8–GFP, 200 μM acetosyringone was added and cells were grown for 24 h at 19 °C. *H. neptunium* ATCC 15444 228405 cells were grown overnight in marine broth (MB) at 30 °C. *C. crescentus* NA1000 565050 cells were synchronized in M2 buffer to get swarmer cells, as described in refs. 38 and 39. *C. jejuni* subspecies *jejuni* 81116 407148 were grown as described in ref. 37. Briefly, cells were grown under microaerobic conditions for 48 to 60 h on Mueller–Hinton (MH) agar using CampyPak sachets (Oxoid) at 37 °C. After that, cultures were restreaked and incubated for an extra 16 h. Then, bacteria were resuspended into 1 mL of MH broth to an OD_{600} of 10 and were subsequently plunge-frozen. *H. gracilis* cells were grown for 48 h in Broth 233 at 26 °C without antibiotics to $OD_{600} < 0.1$. Subsequently, cells were spun down at 1,000 × *g* for 5 min and concentrated by ∼10× for plunge-freezing. *A. longum* were grown anaerobically on rhamnose, as described in ref. 40. Note that some of the cells were grown for purposes other than observing their flagellar systems.

Cryo-ET Sample Preparation and Imaging. The 10- or 20-nm gold beads were first coated with bovine serum albumin, and then the solution was mixed with cells. Three to four microliters of this mixture was applied to a glow-discharged, carbon-coated, R2/2, 200 mesh copper Quantifoil grid (Quantifoil Micro Tools) in a Vitrobot chamber (FEI) with 100% humidity at room temperature. Samples were blotted by using Whatman paper and then plunge-frozen in an ethane/propane mix. Imaging was done on an FEI Polara 300-keV field emission gun electron microscope (FEI) equipped with a Gatan image filter and K2 Summit direct electron detector in counting mode (Gatan). Data were collected by using the University of California San Francisco (UCSF) Tomography software (41) with each tilt series ranging from −60° to 60° in increments ranging from 1° to 3° and an underfocus range of ∼5 to 10 μm for the different samples. A cumulative electron dose of 200 e^-/A^2 for each individual tilt series in *A. longum*, 200 e^-/A^2 for *A. tumefaciens*, 200 e^-/A^2 for *C. crescentus*, 75 e^-/A^2 for *H. gracilis*, 160 e^-/A^2 for *V. cholerae*, 160 e^-/A^2 for *V. harveyi*, 150 e^-/A^2 for *V. fischeri*, 200 e^-/A^2 *H. neptunium*, and 200 e^-/A^2 for *C. jejuni* was used.

Image Processing and Subtomogram Averaging. Three-dimensional reconstructions of the tilt series were either done through the automatic RAPTOR pipeline used in the Jensen laboratory at California Institute of Technology (Caltech) (42) or by using the IMOD software package (43). Subtomogram averages with twofold symmetrization along the particle *y* axis were produced by using the PEET program (44). The number of PL-subcomplexes that were averaged for each species was as follows: 47 particles were averaged for *V. cholerae*, four particles for *V. harveyi*, four particles for *V. fischeri*, six particles for *A. tumefaciens*, four particles for *H. neptunium*, five particles for *C. crescentus*, and eight particles for *H. gracilis*.

Bioinformatics Analysis. An implicit phylogenetic approach was employed to detect the presence or absence of lateral gene transfer of *flgI* or *flgH* between subphyla of bacteria. In this analysis, species distance was estimated from the protein-sequence distance between a set of single-copy cluster of orthologous genes (COGs), and gene distance was estimated from the distance between individual flagellar protein sequences. The set of single-copy COGs was taken from ref. 32 and further refined to only 25 COGs that contained a single copy in all 15 species considered here. These COG proteins along with the flagellar proteins FlgI and FlgH were individually aligned with MUSCLE (45) with 100 maxiters. Conserved blocks were identified by using Gblocks (46) with a maximum of eight contiguous nonconserved positions, a minimum length of two for a block, and half-gap positions allowed, and a similarity matrix was employed. Following the individual processing of the single-copy COGs, the individual multiple sequence alignments (MSAs) were concatenated to create a species-level alignment. Pairwise distances within the MSA of flagellar protein sequences and within the MSA of concatenated single-copy COGs were calculated by using the DistanceMatrix library in Biopython with the BLOSUM62 substitution matrix.

Constructing the Taxonomic Tree. A total of 400 representative bacterial species were selected at random from all bacteria in UniProt with a reference proteome annotation. Species included in this study were appended to this list. The full list of species can be found in *SI Appendix*, Table S7. The taxonomic tree was rendered by using the Environment for Tree Exploration (ETE) (47).

GC-Content Analysis. Fasta files and gff3 files for *S. putrefaciens* and *P. shigelloides* were downloaded from Ensembl Genomes. Gene boundaries were extracted from the gff3 files, and the percent G or C within the coding region was calculated for each gene in the species.

Data Availability. Some of the data used in this study are available in the Electron Tomography Database (ETDB)-Caltech (48). All of the data are available upon request from the corresponding author.

ACKNOWLEDGMENTS. This work was supported by NIH Grant R35 GM122588 (to G.J.J.). Cryo-ET work was done in the Beckman Institute Resource Center for Transmission Electron Microscopy at the California Institute of Technology. M.K. was supported by a Rubicon postdoctoral fellowship from De Nederlandse Organisatie voor Wetenschappelijk Onderzoek. J.P.G.L.M.R. was supported by NIH Grant R35GM122543. Ariane Briegel kindly helped in collecting part of the data. We thank Catherine M. Oikonomou for reading the manuscript and for the insightful discussions; and Dr. Pat Zambryski from the University of California, Berkeley for providing us with the *A. longum* strain used in this study.

1. R. M. Macnab, How bacteria assemble flagella. *Annu. Rev. Microbiol.* **57**, 77–100 (2003).
2. C. J. Jones, R. M. Macnab, Flagellar assembly in *Salmonella typhimurium*: Analysis with temperature-sensitive mutants. *J. Bacteriol.* **172**, 1327–1339 (1990).
3. T. Kubori, N. Shimamoto, S. Yamaguchi, K. Namba, S. Aizawa, Morphological pathway of flagellar assembly in *Salmonella typhimurium*. *J. Mol. Biol.* **226**, 433–446 (1992).
4. H. Li, V. Sourjik, Assembly and stability of flagellar motor in *Escherichia coli*. *Mol. Microbiol.* **80**, 886–899 (2011).
5. F. D. Fabiani *et al*., A flagellum-specific chaperone facilitates assembly of the core type III export apparatus of the bacterial flagellum. *PLoS Biol.* **15**, e2002267 (2017).
6. E. J. Cohen, K. T. Hughes, Rod-to-hook transition for extracellular flagellum assembly is catalyzed by the L-ring-dependent rod scaffold removal. *J. Bacteriol.* **196**, 2387–2395 (2014).
7. M. Kaplan *et al*., In situ imaging of the bacterial flagellar motor disassembly and assembly processes. *EMBO J.* **38**, e100957 (2019).
8. S. Chen *et al*., Structural diversity of bacterial flagellar motors. *EMBO J.* **30**, 2972–2981 (2011).
9. M. Kaplan *et al*., The presence and absence of periplasmic rings in bacterial flagellar motors correlates with stator type. *eLife* **8**, e43487 (2019).
10. Z. Qin, W. T. Lin, S. Zhu, A. T. Franco, J. Liu, Imaging the motility and chemotaxis machineries in *Helicobacter pylori* by cryo-electron tomography. *J. Bacteriol.* **199**, e00695–e16 (2017).
11. X. Zhao, S. J. Norris, J. Liu, Molecular architecture of the bacterial flagellar motor in cells. *Biochemistry* **53**, 4323–4333 (2014).
12. B. Chaban, I. Coleman, M. Beeby, Evolution of higher torque in *Campylobacter*-type bacterial flagellar motors. *Sci. Rep.* **8**, 97 (2018).
13. H. Terashima, H. Fukuoka, T. Yakushi, S. Kojima, M. Homma, The *Vibrio* motor proteins, MotX and MotY, are associated with the basal body of Na-driven flagella and required for stator formation. *Mol. Microbiol.* **62**, 1170–1180 (2006).
14. H. Terashima, M. Koike, S. Kojima, M. Homma, The flagellar basal body-associated protein FlgT is essential for a novel ring structure in the sodium-driven *Vibrio* motor. *J. Bacteriol.* **192**, 5609–5615 (2010).
15. J. M. Skerker, M. T. Laub, Cell-cycle progression and the generation of asymmetry in *Caulobacter crescentus*. *Nat. Rev. Microbiol.* **2**, 325–337 (2004).
16. J. L. Ferreira *et al*., γ-Proteobacteria eject their polar flagella under nutrient depletion, retaining flagellar motor relic structures. *PLoS Biol.* **17**, e3000165 (2019).
17. S. Zhu *et al*., *In situ* structures of polar and lateral flagella revealed by cryo-electron tomography. *J. Bacteriol.* **201**, e00117-19 (2019).
18. X.-Y. Zhuang *et al*., Dynamic production and loss of flagellar filaments during the bacterial life cycle. bioRxiv:10.1101/767319 (27 September 2019).
19. C. M. Oikonomou, G. J. Jensen, A new view into prokaryotic cell biology from electron cryotomography. *Nat. Rev. Microbiol.* **15**, 128 (2017).
20. J. A. G. Briggs, Structural biology in situ—the potential of subtomogram averaging. *Curr. Opin. Struct. Biol.* **23**, 261–267 (2013).
21. K. E. Leigh *et al*., Subtomogram averaging from cryo-electron tomograms. *Methods Cell Biol.* **152**, 217–259 (2019).
22. S. Zhu *et al*., Molecular architecture of the sheathed polar flagellum in *Vibrio alginolyticus*. *Proc. Natl. Acad. Sci. U.S.A.* **114**, 10966–10971 (2017).
23. R. Liu, H. Ochman, Stepwise formation of the bacterial flagellar system. *Proc. Natl. Acad. Sci. U.S.A.* **104**, 7116–7121 (2007).
24. M. Ravenhall, N. Škunca, F. Lassalle, C. Dessimoz, Inferring horizontal gene transfer. *PLOS Comput. Biol.* **11**, e1004095 (2015).
25. E. Cascales, R. Lloubès, J. N. Sturgis, The TolQ-TolR proteins energize TolA and share homologies with the flagellar motor proteins MotA-MotB. *Mol. Microbiol.* **42**, 795–807 (2001).
26. A. Diepold, J. P. Armitage, Type III secretion systems: The bacterial flagellum and the injectisome. *Philos. Trans. R. Soc. Lond. B Biol. Sci.* **370**, 20150020 (2015).
27. M. H. Saier, Jr, Evolution of bacterial type III protein secretion systems. *Trends Microbiol.* **12**, 113–115 (2004).
28. W. Deng *et al*., Assembly, structure, function and regulation of type III secretion systems. *Nat. Rev. Microbiol.* **15**, 323–337 (2017).
29. A. Briegel *et al*., Morphology of the archaellar motor and associated cytoplasmic cone in *Thermococcus kodakaraensis*. *EMBO Rep.* **18**, 1660–1670 (2017).
30. B. Daum *et al*., Structure and *in situ* organisation of the *Pyrococcus furiosus* archaellum machinery. *eLife* **6**, e27470 (2017).
31. S.-V. Albers, K. F. Jarrell, The archaellum: An update on the unique archaeal motility structure. *Trends Microbiol.* **26**, 351–362 (2018).
32. F. D. Ciccarelli *et al*., Toward automatic reconstruction of a highly resolved tree of life. *Science* **311**, 1283–1287 (2006).
33. E. I. Tocheva *et al*., Peptidoglycan remodeling and conversion of an inner membrane into an outer membrane during sporulation. *Cell* **146**, 799–812 (2011).
34. E. I. Tocheva, D. R. Ortega, G. J. Jensen, Sporulation, bacterial cell envelopes and the origin of life. *Nat. Rev. Microbiol.* **14**, 535–542 (2016).
35. D. Oliver, Protein secretion in *Escherichia coli*. *Annu. Rev. Microbiol.* **39**, 615–648 (1985).
36. K. Talmadge, W. Gilbert, Cellular location affects protein stability in *Escherichia coli*. *Proc. Natl. Acad. Sci. U.S.A.* **79**, 1830–1833 (1982).
37. M. Beeby *et al*., Diverse high-torque bacterial flagellar motors assemble wider stator rings using a conserved protein scaffold. *Proc. Natl. Acad. Sci. U.S.A.* **113**, E1917–E1926 (2016).
38. J.-W. Tsai, M. R. K. Alley, Proteolysis of the *Caulobacter* McpA chemoreceptor is cell cycle regulated by a ClpX-dependent pathway. *J. Bacteriol.* **183**, 5001–5007 (2001).
39. A. Briegel *et al*., Multiple large filament bundles observed in *Caulobacter crescentus* by electron cryotomography. *Mol. Microbiol.* **62**, 5–14 (2006).
40. E. I. Tocheva *et al*., Polyphosphate storage during sporulation in the Gram-negative bacterium *Acetonema longum*. *J. Bacteriol.* **195**, 3940–3946 (2013).
41. S. Q. Zheng *et al*., UCSF Tomography: An integrated software suite for real-time electron microscopic tomographic data collection, alignment, and reconstruction. *J. Struct. Biol.* **157**, 138–147 (2007).
42. H. J. Ding, C. M. Oikonomou, G. J. Jensen, The Caltech Tomography Database and automatic processing pipeline. *J. Struct. Biol.* **192**, 279–286 (2015).
43. J. R. Kremer, D. N. Mastronarde, J. R. McIntosh, Computer visualization of three-dimensional image data using IMOD. *J. Struct. Biol.* **116**, 71–76 (1996).
44. D. Nicastro *et al*., The molecular architecture of axonemes revealed by cryoelectron tomography. *Science* **313**, 944–948 (2006).
45. R. C. Edgar, MUSCLE: Multiple sequence alignment with high accuracy and high throughput. *Nucleic Acids Res.* **32**, 1792–1797 (2004).
46. G. Talavera, J. Castresana, Improvement of phylogenies after removing divergent and ambiguously aligned blocks from protein sequence alignments. *Syst. Biol.* **56**, 564–577 (2007).
47. J. Huerta-Cepas, F. Serra, P. Bork, ETE 3: Reconstruction, analysis, and visualization of phylogenomic data. *Mol. Biol. Evol.* **33**, 1635–1638 (2016).
48. D. R. Ortega *et al*., ETDB-Caltech: A blockchain-based distributed public database for electron tomography. *PLoS One* **14**, e0215531 (2019).